Fractal butterflies of chiral fermions in bilayer graphene: Phase transitions and emergent properties

Areg Ghazaryan and Tapash Chakraborty[*]

Department of Physics and Astronomy, University of Manitoba, Winnipeg, Manitoba, Canada R3T 2N2

We have studied the influence of electron-electron interaction on the fractal butterfly spectrum of Dirac fermions in biased bilayer graphene in the fractional quantum Hall effect (FQHE) regime. We demonstrate that the butterfly spectrum exhibits remarkable phase transitions between the FQHE gap and the butterfly gap for chiral electrons in bilayer graphene, when the periodic potential strength or the bias voltage is varied. We also find that, in addition to those phase transitions, by varying the bias voltage one can effectively control the periodic potential strength experienced by the electrons. The electron-electron interaction causes the butterfly spectrum to exhibit new gaps inside the Bloch sub-bands not found in the single-particle case. We expect that both the observed phase transition and other new features in the butterfly spectrum of interacting Dirac fermions will be of great interest to researchers from diverse fields.

　　　　PACS number(s): 73.22.−f, 71.10.Pm, 73.43.−f

I. INTRODUCTION

The dynamics of an electron on a two-dimensional periodic lattice subjected to a magnetic field has been of interest in physics and mathematics for several decades. The eponymous Harper introduced in 1955 [1] the Hamiltonian for a Bloch particle on a square lattice in a magnetic field, the solution of which [2] resulted in the famous Hofstadter butterfly spectrum. One of the most interesting features of the spectrum is its self-similar nature, indicating that it is a member of the class of fractal patterns. The Harper equation has been extensively studied in mathematics, where a rigorous mathematical proof that the Hofstadter butterfly is a representative of a Cantor set and therefore is a fractal spectrum has been presented (the so-called ten Martini problem) [3]. In the field of physics, the butterfly spectrum has been viewed as the quantum phase diagram with infinitely many phases [4]. There were several attempts to realize the butterfly spectrum experimentally in many branches of physics, viz., optics [5], acoustics [6], cold atoms [7], and nanoscale superlattices [8]. Finally, in 2013, monolayer or bilayer graphene [9,10] placed on a hexagonal boron nitride substrate with rotational misalignment between graphene and the substrate revealed the unique fractal pattern of the butterflies [11–13] in the energy spectrum of noninteracting Dirac fermions. That particular arrangement of graphene on the substrate resulted in the moiré pattern, which actually introduces a large-scale periodicity in the Hamiltonian of the system, and the fractal butterfly pattern was the result of splitting of the moiré minibands (secondary Dirac cones) by the magnetic field that are exhibited in the magnetoconductance probe [14]. After that exciting experimental discovery of the fractal butterflies, more recent studies (both theoretical [15] and experimental [16]) have focused on the influence of the electron-electron interaction on the butterfly spectrum. Electronic properties of Dirac fermions in monolayer and bilayer graphene have been exhaustively studied in recent years [9,10,17]. In a strong perpendicular magnetic field, interacting Dirac fermions [18] display the fractional quantum Hall Effect (FQHE) states [19] in monolayer [20]

and bilayer graphene [17,21], that has also been experimentally observed [22]. The interaction effects in the fractal butterflies are, of course, more complex in the fractional quantum Hall effect regime, where one observes an interplay between the quantum Hall effect gap and the Hofstadter gap [23].

Interestingly, in this work we find that the butterfly spectra exhibit remarkable phase transitions for chiral electrons in bilayer graphene. We found that bilayer graphene has the unique advantage that it offers the possibility to essentially control the periodic potential strength via the bias voltage and therefore control the transition between two quantum phases. At small values of the periodic potential strength, the system can be described as interacting electrons in high magnetic fields and therefore we enter the regime of the FQHE. By increasing the periodic potential strength, we observe a phase transition into the Hofstadter butterfly spectrum which now includes the electron-electron interaction. The important observation of our present work is that the electron-electron interaction results in the generation of new gaps in the butterfly spectrum inside the Bloch sub-bands, not expected in the single-particle case. This has important implications for experimental observation of these effects in graphene butterflies [24]. Our prediction (and eventual experimental confirmation) of new quantum phase transitions in the FQHE regime will be interesting for researchers in various subfields of physics. For example, as the interaction effects can be investigated experimentally for cold atoms in optical lattices, our predictions will perhaps motivate further experiments in that direction [7]. Our work will also be of interest to researchers active in the field of quantum Hall effect, as it will extend previous studies of quantum phase transitions in the integer quantum Hall effects [4] to the FQHE regime. Of course, it will also be interesting for researchers working with graphene superlattices on top of the hexagonal boron nitride [24].

II. THEORETICAL FRAMEWORK

We consider bilayer graphene with Bernal (AB) stacking in an external periodic potential with square symmetry [15,25–27]. We label the layers of bilayer graphene by the indices 1 and 2 and assume that the periodic potential is present only

―――――
[*]tapash.chakraborty@umanitoba.ca

in layer 1. The single-particle Hamiltonian in a magnetic field (without the periodic potential) is written [9,10,17,28]

$$
\mathcal{H}_\xi^{bi} = \xi \begin{pmatrix} \frac{U}{2} & v_F \pi_- & 0 & 0 \\ v_F \pi_+ & \frac{U}{2} & \xi \gamma_1 & 0 \\ 0 & \xi \gamma_1 & -\frac{U}{2} & v_F \pi_- \\ 0 & 0 & v_F \pi_+ & -\frac{U}{2} \end{pmatrix}, \quad (1)
$$

where $\pi_\pm = \pi_x \pm i\pi_y$, $\boldsymbol{\pi} = \mathbf{p} + e\mathbf{A}/c$, $\mathbf{p}$ is the two-dimensional electron momentum, $\mathbf{A} = (0, Bx, 0)$ is the vector potential, $v_F \approx 10^6$ m/s is the Fermi velocity in graphene, U is the interlayer bias voltage, $\gamma_1 \approx 0.4$ eV is the interlayer hopping integral, and $\xi = 1$ for the K valley and $\xi = -1$ for the K' valley. The corresponding wave function is described by a four-component spinor $(\psi_{A_1}, \psi_{B_1}, \psi_{A_2}, \psi_{B_2})^T$ for valley K and $(\psi_{B_2}, \psi_{A_2}, \psi_{B_1}, \psi_{A_1})^T$ for valley K', where ψ_A and ψ_B are wave functions of sublattices A and B, respectively. We consider the fully spin-polarized electron system and therefore disregard the Zeeman energy. The eigenfunction of the Hamiltonian (1) then has the form

$$
\Psi_{n,j} = \begin{pmatrix} \xi C_1 \varphi_{n-1,j} \\ C_2 \varphi_{n,j} \\ C_3 \varphi_{n,j} \\ \xi C_4 \varphi_{n+1,j} \end{pmatrix}, \quad (2)
$$

where C_1, C_2, C_3, C_4 are constants and $\varphi_{n,j}$ is the electron wave function in the nth Landau level (LL) with the parabolic dispersion, taking into account the periodic boundary conditions (PBCs) [19,29]:

$$
\varphi_{n,j}(x,y) = \frac{1}{\sqrt{L_y \pi^{1/2} \ell_0 2^n n!}} \sum_{k=-\infty}^{\infty} e^{\frac{i}{\ell_0^2}(X_j + kL_x)y}
$$
$$
\times e^{-\frac{(x+kL_x+X_j)^2}{2\ell_0^2}} H_n\left(\frac{x+kL_x+X_j}{\ell_0}\right), \quad (3)
$$

where $X_j = 2\pi j \ell_0^2/L_y$, $\ell_0 = \sqrt{c\hbar/eB}$ is the magnetic length, $H_n(x)$ are the Hermite polynomials, and L_x and L_y describe the size of the system. In the wave function (2) the LL index n can take the values $-1, 0, 1, \ldots$ and we assume that if the LL index of $\varphi_{n,j}$ is negative then it is identically equal to zero. Then, for $n = -1$ the wave function (2) is $\Psi_{-1,j} = (0, 0, 0, \varphi_{0,j})$ and there is only one energy level corresponding to this case. For $n = 0$, $C_1 = 0$ and there are three energy states. Following the convention for indexing the energy levels introduced in Ref. [17], we label the states for $n = -1$ and 0 as $0_i^{(\xi)}$, where $i = -2, -1, 1, 2$ is the label of states in ascending order of the energy values. In particular, for valley K the state corresponding to $n = -1$ has the index $0_{-1}^{(+)}$ and $0_1^{(-)}$ for valley K'.

The complete many-body Hamiltonian for this system can be written as

$$
\mathcal{H} = \sum_i^{N_e} \left[\mathcal{H}_\xi^{bi} + V(x_i, y_i) \right] + \frac{1}{2} \sum_{i \neq j}^{N_e} V_{ij}. \quad (4)
$$

Here the second term is the periodic potential, which is nonzero only for the components of layer 1 and has the form

$$
V(x,y) = V_0[\cos(q_x x) + \cos(q_y y)], \quad (5)
$$

where V_0 is the amplitude of the periodic potential and $q_x = q_y = q_0 = 2\pi/a_0$, where a_0 is the period of the external potential. The last term in Eq. (4) is the Coulomb interaction. Defining the parameter $\alpha = \phi_0/\phi$ (the inverse of the magnetic flux through the unit cell measured in units of the flux quantum), where $\phi = Ba_0^2$ is the magnetic flux through the unit cell of the periodic potential and $\phi_0 = hc/e$ is the flux quantum, we consider two magnetic field strength values in this work corresponding to $\alpha = 1/2$ and $1/3$. The Coulomb interaction energy ($\approx e^2/\varepsilon \ell_0$) is around 102 meV for $\alpha = 1/2$ and 125 meV for $\alpha = 1/3$, whereas the LL separation is of the order of 200 meV for these magnetic field strengths. As shown below the Hofstadter gap is around 5 meV for $\alpha = 1/2$ and 11 meV for $\alpha = 1/3$ and is comparable to or larger than the FQHE gap for 1/3 filling (around 4 meV). This means that the valley mixing terms due to the Coulomb interaction and the warping terms due to the band structure of bilayer graphene [9] will have similar or even less impact on the Hofstadter gap compared to the FQHE gap. Therefore we can ignore them in our calculations, based on the results for the FQHE gap [17,21]. As for the valley mixing due to the periodic potential, it is expected to be extremely small due to the two orders of difference between the periodic potential lattice constant and the bilayer graphene lattice constant [23,30]. Therefore we ignore the valley mixing due to the periodic potential as well. Both the interlayer bias voltage and the periodic potential break spatial inversion symmetry and therefore the valley degeneracy is lifted in this system [31].

For the many-body problem we consider a system of finite number N_e of electrons in a toroidal geometry, i.e., the size of the system is $L_x = M_x a_0$ and $L_y = M_y a_0$ (M_x and M_y are integers), and we apply PBCs in order to eliminate the boundary effects. It can be deduced that $N_s/(M_x M_y) = 1/\alpha$, where N_s is the number of magnetic flux quanta passing through the system or, alternatively, it describes the LL degeneracy for each value of the spin and valley index and takes integer values. The filling factor is defined as $\nu = p/q = N_e/N_s$, where p and q are again coprime integers. In order to solve this problem we first construct the Hamiltonian matrix using the Hamiltonian operator (4) and the many-body states $|j_1, j_2, \ldots, j_{N_e}\rangle$ (besides j_i, each single-particle state is characterized by the LL and valley indices which are not shown, but are implicitly assumed to be included in the indices j_i) which are constructed from the single-particle eigenvectors (2). After that we use the translational symmetry of the system to reduce the size of the Hilbert space. It is easy to show [19,23,30,32,33] that the translations which commute with the many-body Hamiltonian (4) and also respect the imposed PBC are the center-of-mass (CM) translation operators defined as

$$
T^{CM}(\mathbf{a}) = \prod_{i=1}^{N_e} T_i(\mathbf{a}) \quad (6)
$$

with the translation of the form $\mathbf{a}_p = m\beta_1 a_0 \hat{\mathbf{x}} + n\beta_2 a_0 \hat{\mathbf{y}}$. Here $T_i(\mathbf{a})$ is the single-particle translation operator, m and n are integers which characterize the translation vector $\mathbf{a}_p$, and β_1 and β_2 are again integers which are determined from the condition that the CM translation operators should commute with each other for different values of m and n. $\beta_1 \beta_2$ describes

the degeneracy of the states characterized with the same eigenvalue of the CM translation operator. The eigenvalues of the CM translation operator are defined through the CM momentum of the system, and therefore this approach also makes it possible to characterize each eigenstate of the system with its CM momentum. It can be shown [19,30] that the eigenstates of the CM translation operator have the form

$$|(s,t)\rangle = \frac{1}{\sqrt{|\mathcal{L}|}} \sum_{k=0}^{|\mathcal{L}|-1} e^{-i2\pi \frac{\beta_1 s}{M_x} k}$$
$$\times |j_1 + \beta_1 \kappa_x k, j_2 + \beta_1 \kappa_x k, \ldots, j_{N_e} + \beta_1 \kappa_x k\rangle, \quad (7)$$

where s and t are integers defined modulo M_x/β_1 and M_y/β_2, respectively, and characterize both the eigenvalues of $T^{\text{CM}}(\mathbf{a})$ and CM momentum of the system. κ_x is an integer defined through the relation $N_s = \kappa_x M_x$ and $|\mathcal{L}|$ defines the size of the set $\mathcal{L}$ which is the set of the states related to each other by the relation

$$|j'_1, j'_2, \ldots, j'_{N_e}\rangle = |j_1 + k\beta_1 \kappa_x, j_2 + k\beta_1 \kappa_x, \ldots, j_{N_e} + k\beta_1 \kappa_x\rangle, \quad (8)$$

which is finite because j_i are defined modulo N_s. Using the eigenstates (7) the complete Hamiltonian matrix of the many-body system can be brought into the block-diagonal form, where each block can then be diagonalized using the exact diagonalization procedure.

III. RESULTS AND DISCUSSION

In this work we consider the filling factor $\nu = 1/3$ for a fully spin-polarized system and for $\alpha = 1/2$ and $1/3$. The period of the external potential is taken to be $a_0 = 20$ nm, and the interlayer hopping integral is taken to be $\gamma_1 = 30$ meV [21], which can be achieved by applying an in-plane magnetic field [17]. The number of many-body basis states $|j_1, j_2, \ldots, j_{N_e}\rangle$ is determined by the binomial coefficient $C_{N_s}^{N_e}$, which is 495 for $N_e = 4$, 18 564 for $N_e = 6$, and 735 471 for $N_e = 8$ for the filling factor considered in this work. As was noted above using the CM translation algebra the complete Hamiltonian matrix can be brought into the block-diagonal form where each block size is $\beta_1 \beta_2 C_{N_s}^{N_e}/M_x M_y$. For the values of α considered in this work β_1 and β_2 can be chosen to be equal to 1 [30] and $M_x M_y$ can be determined from the equation $M_x M_y = N_s \alpha$. For example, for $N_e = 6$ the $M_x M_y = 9$ for $\alpha = 1/2$ and $M_x M_y = 6$ for $\alpha = 1/3$. This matrix size reduction is smaller than for the case of the system without a periodic potential, where the relative translation algebra can be used to reduce the size of the block to $p^2 C_{N_s}^{N_e}/N_e^2$ [19]. Due to this major disadvantage in the present case and also due to the additional nonzero matrix elements in the presence of the periodic potential, evaluation of energy levels for $N_e = 8$ becomes considerably complicated. Therefore we consider in this work systems comprising up to $N_e = 6$ electrons.

In Fig. 1 the regions of the bias voltage where the gap corresponds to the butterfly region or the FQHE region for $N_e = 4$ (a,c) and $N_e = 6$ (b,d) for LL $0_i^{(+)}$ are presented by the color of filled dots. The filled dots are figuratively plotted on top of the dependence of LLs on the bias voltage, which
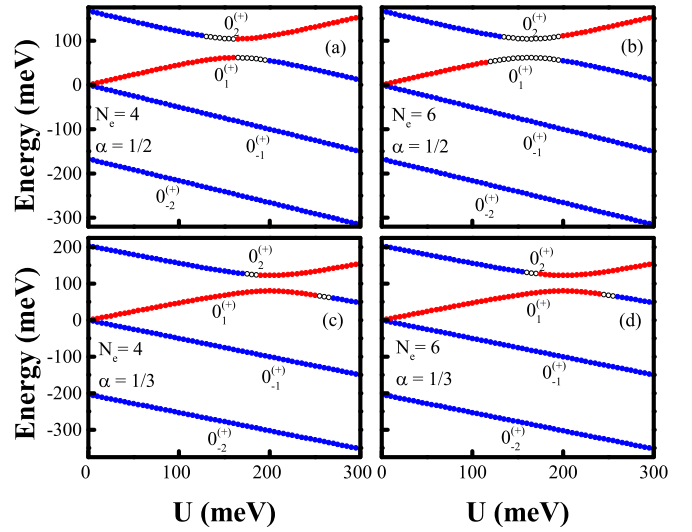
FIG. 1. (Color online) The Landau levels for $n = -1$ and 0 vs the bias voltage U for two values of α without taking into account the periodic potential. The numbers next to the curves denote the corresponding Landau level as described in the text. The regions where the gap corresponds to the FQHE (butterfly) gap are drawn as blue (red) dots. Results in (a) and (c) are for $N_e = 4$ while those in (b) and (d) are for $N_e = 6$. In the FQHE and butterfly gap calculations the periodic potential strength is $V_0 = 20$ meV.

does not take the periodic potential into account. The periodic potential strength V_0 is taken to be $V_0 = 20$ meV. In order to understand the phase transitions observed in Fig. 1 the wave functions and also the impact of the bias voltage on these wave functions should be analyzed for each LL. As mentioned above, for level $0_{-1}^{(+)}$ the wave function has a nonzero component only in layer 2 and this remains true for all values of the bias voltage. Due to the fact that the periodic potential is present only in the first layer, the wave functions and therefore also the FQHE gaps do not depend on the bias voltage for LL $0_{-2}^{(+)}$ and there is no phase transition. In the LL $0_{-1}^{(+)}$, for $U = 0$ the electrons are mostly located in layer 2, although they have small probability of being in layer 1. Increasing the bias voltage, both the single-particle and the many-particle system become even more polarized in layer 2, and therefore the periodic potential has a negligible impact on this level as well and we observe the FQHE gap for all values of U. The situation is different for LL $0_1^{(+)}$ and $0_2^{(+)}$. For $U = 0$ the electrons in $0_1^{(+)}$ are mostly localized in layer 1 and therefore the periodic potential has a drastic impact in this case.

In monolayer graphene the magnitude of the periodic potential $V_0 = 20$ meV for $N_e = 4$ and 6 and for both values of α closes the FQHE gap and opens the butterfly gap [23]. It should be pointed out that for $\alpha = 1/2$ there is no gap in the butterfly spectrum for noninteracting electrons, but the electron-electron interaction opens a gap [15]. However, for $\alpha = 1/3$ the gap is due to both the Hofstadter gap observed in the single-particle case and the contribution from the electron-electron interaction. Therefore, the gap for LL $0_1^{(+)}$ corresponds to the butterfly gap for low values of the bias voltage U. The electrons in $0_2^{(+)}$ are mostly localized in layer 2 and therefore the periodic potential has only a minor effect on
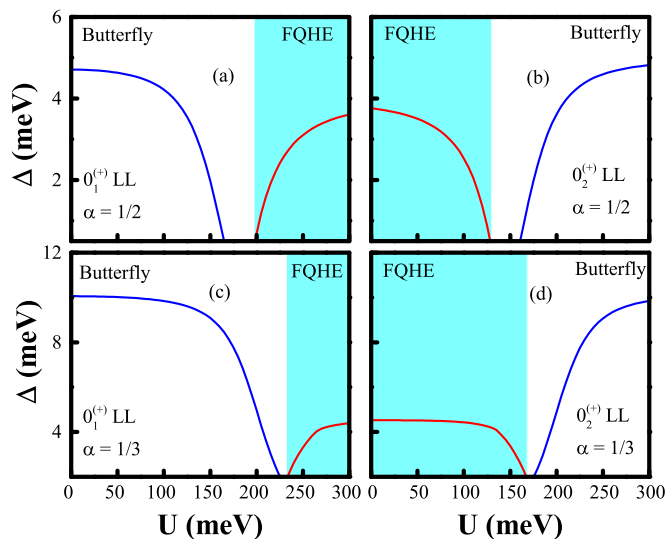
FIG. 2. (Color online) The dependence of FQHE and butterfly gaps for $N_e = 4$ electrons on the bias voltage U and the Landau levels $0_1^{(+)}$ and $0_2^{(+)}$ for two values of α, with the periodic potential strength $V_0 = 20$ meV. The line corresponding to the FQHE (butterfly) case is depicted in red (blue). The region of the bias voltage U where the gap corresponds to the FQHE gap is marked in cyan.

FIG. 3. (Color online) The dependence of FQHE and butterfly gaps for $N_e = 4$ electrons on the periodic potential strength V_0 for Landau levels $0_1^{(+)}$ and $0_2^{(+)}$ and for the bias voltages $U = 0$ and 200 meV, and $\alpha = 1/2$. The line corresponding to the FQHE (butterfly) is depicted in red (blue). The region of the periodic potential strength V_0 where the gap corresponds to the FQHE gap is marked in cyan.

them. Hence for the $0_2^{(+)}$ LL the FQHE gap is observed for low values of the bias voltage U. By increasing the bias voltage U there is an anticrossing between these two LLs ($0_1^{(+)}$ and $0_2^{(+)}$) and thereafter the layer polarization in each LL changes drastically. In particular, for the LL $0_1^{(+)}$ at the bias voltage $U = 250$ meV the probabilities of electrons being localized in layer 2 and of the electrons in LL $0_2^{(+)}$ being localized in layer 1 are already ≈ 0.95. This results in a phase transition in both LLs; namely, the gap in the LL $0_1^{(+)}$ which initially represented the butterfly gap now corresponds to the FQHE gap. The opposite behavior occurs for the LL $0_2^{(+)}$.

The closure of the FQHE gap by the external periodic potential also occurs in monolayer graphene [23]. However, in bilayer graphene one can control the actual strength of the periodic potential experienced by the electrons essentially by applying the bias voltage. The implications of this interesting result will be discussed below. The described behavior is almost the same for both values of $\alpha = 1/2$ and $1/3$. The essential difference between these two cases is that the butterfly gap for $\alpha = 1/3$ is substantially bigger than that for $\alpha = 1/2$. Therefore the bias voltage U required to observe the phase transition from the butterfly region to the FQHE region for the LL $0_1^{(+)}$ is bigger for $\alpha = 1/3$ than for $\alpha = 1/2$. Similar studies for the K' valley exhibit the same phase transitions for the LLs $0_{-2}^{(-)}$ and $0_{-1}^{(-)}$ in the negative energy region.

In Fig. 2, the dependence of both the FQHE and the butterfly gaps for $N_e = 4$ electrons on the bias voltage U for Landau levels $0_1^{(+)}$ and $0_2^{(+)}$ and for two values of α is shown for $V_0 = 20$ meV. The region of the bias voltage U where the gap corresponds to the FQHE and the butterfly gap is also indicated. As was already pointed out, the layer polarization of the electrons changes drastically near the anticrossing point of the LLs $0_1^{(+)}$ and $0_2^{(+)}$ and the consequence of that can be
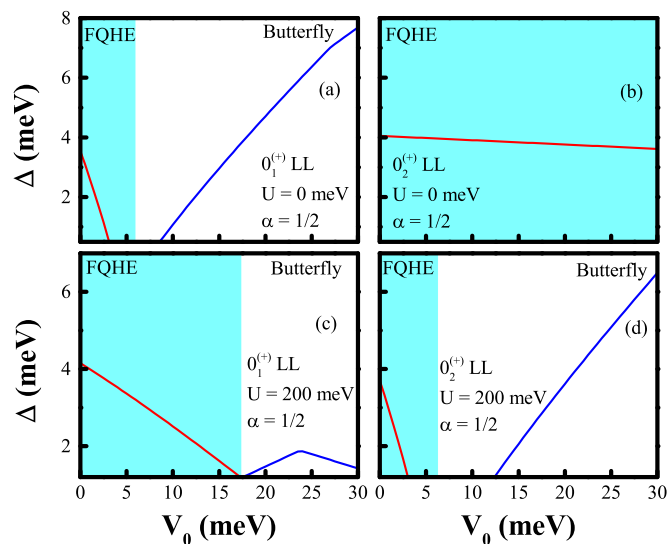
clearly seen in the dependence of the gaps on the bias voltage U. In Fig. 2, in the regions further away from the anticrossing point the gaps are almost constant and fall rapidly to zero when approaching the anticrossing point. Also it can be clearly seen that the FQHE gap is almost the same for both LLs and for both values of α, whereas the butterfly gap is almost twice as big for $\alpha = 1/3$ compared to that of $\alpha = 1/2$ as explained above.

The dependence of both the FQHE and the butterfly gaps for $N_e = 4$ electrons on the periodic potential strength V_0 for Landau levels $0_1^{(+)}$ and $0_2^{(+)}$ is shown in Fig. 3 for the bias voltages $U = 0$ and 200 meV, and for $\alpha = 1/2$. The same dependence for $\alpha = 1/3$ is shown in Fig. 4. The region of the periodic potential strength V_0 where the gap corresponds to the FQHE and the butterfly gaps is also indicated. In Figs. 3 and 4, similar phase transitions between the FQHE and the butterfly gaps are observed as well, although the dependence of the gap on the periodic potential strength V_0 is almost linear in comparison to the dependence on the bias voltage U. No phase transition is observed for the LL $0_2^{(+)}$ and $U = 0$ meV, because as was noted above in this case the electrons are mostly localized in layer 2 and the periodic potential has almost no impact on the physical system. This feature is not observed for $U = 200$ meV, because as we noted above application of a bias voltage gradually polarizes the electrons for the LL $0_2^{(+)}$ from layer 2 to layer 1 and the effect of the periodic potential is apparent already for $U = 200$ meV. A similar behavior is observed for LL $0_1^{(+)}$, where the application of the bias voltage results in widening of the FQHE gap region for both values of α. While the butterfly gap is almost linear for $\alpha = 1/3$ in Fig. 4, which indicates that the main contribution here is due to the Hofstadter gap (single particle), for $\alpha = 1/2$ (Fig. 3) it
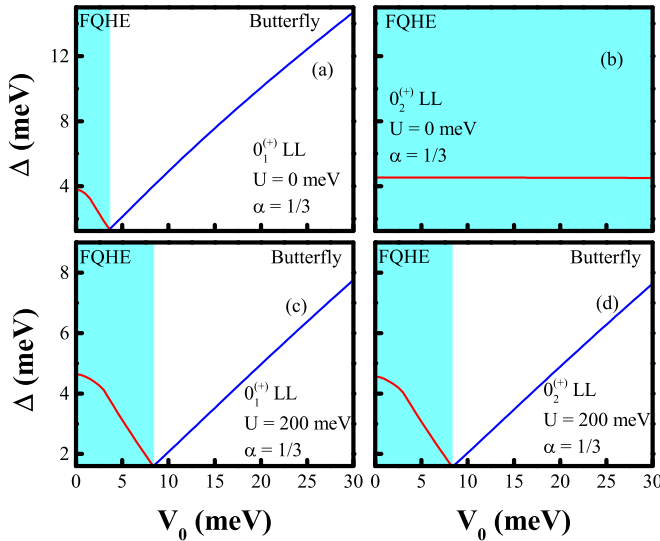
FIG. 4. (Color online) Same as in Fig. 3 but for $\alpha = 1/3$.

deviates from the linear behavior in some cases. This indicates that the butterfly gap due to the interaction is highly nontrivial.

While the closure of the FQHE gap and opening of the butterfly gap due to the external periodic potential occurs in monolayer graphene [23], one cannot control the periodic potential strength in that system. Therefore, there is no direct means to vary the periodic potential strength in the experiment. Our work indicates that in bilayer graphene this is achieved by applying a bias voltage on the sample. In fact, the variation of the bias voltage offers us the ability to control the polarization of the electrons between the two layers, which essentially translates to the control of the strength of the periodic potential. Further, it also exhibits the phase transition between the FQHE gap and the butterfly gap. The obtained phase transitions can be observed through Hall conductance measurements on bilayer graphene placed on a hexagonal boron nitride substrate.

By changing the bias voltage potential from 0 to 300 meV and keeping the electron density unchanged the transitions between the fractional (corresponding to the FQHE gap) [19] and the integer (corresponding to the butterfly gap) [34] Hall conductances could possibly be observed in the experiment. Therefore the obtained results of the current paper can have significant implications for experimental realization of the fractal butterflies in the FQHE regime.

IV. CONCLUSION

In conclusion, we have utilized the exact diagonalization scheme to study the FQHE and the butterfly gaps in bilayer graphene in the presence of the applied interlayer bias voltage and for the filling factor $\nu = 1/3$. We have considered the case when the external periodic potential is present in one layer and have illustrated the effect of varying both the periodic potential strength and the bias voltage on the FQHE and the butterfly gaps. Two values of the parameter α were considered, namely, $\alpha = 1/2$ and $1/3$. We found that by varying either the periodic potential strength or the bias voltage for some Landau levels in both valleys a phase transition from the FQHE gap to the butterfly gap or vice versa can be observed. While the periodic potential strength is characteristic of the sample used in the experiment and cannot be varied directly, our finding shows that, by varying the bias voltage, change of the periodic potential strength actually experienced by the electrons can be achieved, which can have a huge impact on the experimental investigation of the fractal butterflies in the FQHE region.

[1] P. G. Harper, Proc. Phys. Soc. A **68**, 874 (1955).

[2] D. Hofstadter, Phys. Rev. B **14**, 2239 (1976); see also M. Y. Azbel, Sov. Phys. JETP **19**, 634 (1964); D. Langbein, Phys. Rev. **180**, 633 (1969).

[3] A. Avila and S. Jitomirskaya, Ann. Math. **170**, 303 (2009); in *Mathematical Physics of Quantum Mechanics*, edited by J. Asch and A. Joye (Springer, Berlin, 2006), Ch. 1, pp. 5–16.

[4] D. Osadchy and J. E. Avron, J. Math. Phys. **42**, 5665 (2001).

[5] U. Kuhl and H.-J. Stöckmann, Phys. Rev. Lett. **80**, 3232 (1998).

[6] O. Richoux and V. Pagneux, Europhys. Lett. **59**, 34 (2002).

[7] M. Aidelsburger, M. Atala, M. Lohse, J. T. Barreiro, B. Paredes, and I. Bloch, Phys. Rev. Lett. **111**, 185301 (2013); H. Miyake, G. A. Siviloglou, C. J. Kennedy, W. C. Burton, and W. Ketterle, *ibid.* **111**, 185302 (2013).

[8] For earlier experimental attempts in semiconductors, see, for example, M. C. Geisler, J. H. Smet, V. Umansky, K. von Klitzing, B. Naundorf, R. Ketzmerick, and H. Schweizer, Phys. Rev. Lett. **92**, 256801 (2004); Physica E **25**, 227 (2004); C. Albrecht, J. H. Smet, K. von Klitzing, D. Weiss, V. Umansky, and H. Schweizer, Phys. Rev. Lett. **86**, 147 (2001); Physica E **20**, 143 (2003);

T. Schlösser, K. Ensslin, J. P. Kotthaus, and M. Holland, Europhys. Lett. **33**, 683 (1996); Semicond. Sci. Technol. **11**, 1582 (1996).

[9] *Physics of Graphene*, edited by H. Aoki and M. S. Dresselhaus (Springer, New York, 2014).

[10] D. S. L. Abergel, V. Apalkov, J. Berashevich, K. Ziegler, and T. Chakraborty, Adv. Phys. **59**, 261 (2010).

[11] C. R. Dean, L. Wang, P. Maher, C. Forsythe, F. Ghahari, Y. Gao, J. Katoch, M. Ishigami, P. Moon, M. Koshino, T. Taniguchi, K. Watanabe, K. L. Shepard, J. Hone, and P. Kim, Nature (London) **497**, 598 (2013).

[12] B. Hunt, J. D. Sanchez-Yamagishi, A. F. Young, M. Yankowitz, B. J. LeRoy, K. Watanabe, T. Taniguchi, P. Moon, M. Koshino, P. Jarillo-Herrero, and R. C. Ashoori, Science **340**, 1427 (2013).

[13] L. A. Ponomarenko, R. V. Gorbachev, G. L. Yu, D. C. Elias, R. Jalil, A. A. Patel, A. Mishchenko, A. S. Mayorov, C. R. Woods, J. R. Wallbank, M. Mucha-Kruczynski, B. A. Piot, M. Potemski, I. V. Grigorieva, K. S. Novoselov, F. Guinea, V. I. Falko, and A. K. Geim, Nature (London) **497**, 594 (2013).

[14] For a brief review on fractal butterflies in monolayer and bilayer graphene, see T. Chakraborty and V. M. Apalkov, IET Circuits Devices Syst. **9**, 19 (2015); arXiv:1408.4485.

[15] V. M. Apalkov and T. Chakraborty, Phys. Rev. Lett. **112**, 176401 (2014).

[16] G. L. Yu, R. V. Gorbachev, J. S. Tu, A. V. Kretinin, Y. Cao, R. Jalil, F. Withers, L. A. Ponomarenko, B. A. Piot, M. Potemski, D. C. Elias, X. Chen, K. Watanabe, T. Taniguchi, I. V. Grigorieva, K. S. Novoselov, V. I. Falko, A. K. Geim, and A. Mishchenko, Nat. Phys. **10**, 525 (2014).

[17] T. Chakraborty and V. Apalkov, in Ref. [9], Ch. 8; T. Chakraborty and V. M. Apalkov, Solid State Commun. **175**, 123 (2013).

[18] V. Apalkov and T. Chakraborty, Solid State Commun. **177**, 128 (2014); D. S. L. Abergel and T. Chakraborty, Phys. Rev. Lett. **102**, 056807 (2009); D. S. L. Abergel, V. M. Apalkov, and T. Chakraborty, Phys. Rev. B **78**, 193405 (2008); D. S. L. Abergel, P. Pietiläinen, and T. Chakraborty, *ibid.* **80**, 081408 (2009); V. M. Apalkov and T. Chakraborty, *ibid.* **86**, 035401 (2012).

[19] T. Chakraborty and P. Pietiläinen, *The Quantum Hall Effects* (Springer, New York, 1995); *The Fractional Quantum Hall Effect* (Springer, New York, 1988).

[20] V. M. Apalkov and T. Chakraborty, Phys. Rev. Lett. **97**, 126801 (2006).

[21] V. M. Apalkov and T. Chakraborty, Phys. Rev. Lett. **105**, 036801 (2010); **107**, 186803 (2011).

[22] X. Du, I. Skachko, F. Duerr, A. Luican, and E. Y. Andrei, Nature (London) **462**. 192 (2009); D. A. Abanin, I. Skachko, X. Du, E. Y. Andrei, and L. S. Levitov, Phys. Rev. B **81**, 115410 (2010); K. I. Bolotin, F. Ghahari, M. D. Shulman, H. L. Störmer, and P. Kim, Nature (London) **462**, 196 (2009); F. Ghahari, Y. Zhao, P. Cadden-Zimansky, K. Bolotin, and P. Kim, Phys. Rev. Lett. **106**, 046801 (2011).

[23] A. Ghazaryan, T. Chakraborty, and P. Pietiläinen, J. Phys. Condens. Matter **27**, 185301 (2015).

[24] C. R. Dean (private communication); L. Wang, Y. Gao, B. Wen, Z. Han, T. Taniguchi, K. Watanabe, M. Koshino, J. Hone, and C. R. Dean, arXiv:1505.07180.

[25] U. Rössler and M. Shurke, in *Advances in Solid State Physics*, edited by B. Kramer (Springer, Berlin, 2000), Vol. 40, pp. 35–50.

[26] V. Gudmundsson and R. R. Gerhardts, Surf. Sci. **361**, 505 (1996); Phys. Rev. B **52**, 16744 (1995); **54**, R5223(R) (1996).

[27] M. Koshino and T. Ando, J. Phys. Soc. Jpn **73**, 3243 (2004).

[28] E. McCann and V. I. Falko, Phys. Rev. Lett. **96**, 086805 (2006); E. McCann, Phys. Rev. B **74**, 161403 (2006); E. McCann and M. Koshino, Rep. Prog. Phys. **76**, 056503 (2013).

[29] The periodic rectangular geometry was extensively used earlier in the study of the FQHE in various situations. For example, see T. Chakraborty, Surf. Sci. **229**, 16 (1990); Adv. Phys. **49**, 959 (2000); T. Chakraborty and P. Pietiläinen, Phys. Rev. Lett. **76**, 4018 (1996); **83**, 5559 (1999); Phys. Rev. B **39**, 7971 (1989); V. M. Apalkov, T. Chakraborty, P. Pietiläinen, and K. Niemela, Phys. Rev. Lett. **86**, 1311 (2001); T. Chakraborty, P. Pietiläinen, and F. C. Zhang, *ibid.* **57**, 130 (1986); T. Chakraborty and F. C. Zhang, Phys. Rev. B **29**, 7032(R) (1984); F. C. Zhang and T. Chakraborty, *ibid.* **30**, 7320(R) (1984).

[30] A. Ghazaryan and T. Chakraborty, Phys. Rev. B **91**, 125131 (2015).

[31] M. Koshino and E. McCann, Phys. Rev. B **81**, 115315 (2010); P. Moon and M. Koshino, *ibid.* **90**, 155406 (2014).

[32] F. D. M. Haldane, Phys. Rev. Lett. **55**, 2095 (1985).

[33] A. Kol and N. Read, Phys. Rev. B **48**, 8890 (1993).

[34] D. J. Thouless, M. Kohmoto, M. P. Nightingale, and M. den Nijs, Phys. Rev. Lett. **49**, 405 (1982).